Optimal Trajectory Determination for Increased Relative Navigation Observability of Air Vehicles

Adam M. Fosbury*

Air Force Research Laboratory, Space Vehicles Directorate, Kirtland Air Force Base, NM 87117

John L. Crassidis†

University at Buffalo, State University of New York, Amherst, NY 14260-4400

This paper first derives the full equations of motion for relative navigation of air vehicles. An extended Kalman filter is used for estimating the relative position and attitude of two air vehicles, designated leader and follower. All leader states are assumed known, while the relative states are estimated using line-of-sight measurements between the vehicles along with acceleration and angular rate measurements of the follower. Noise is present on all measurements, while biases are present only on the latter two. The global attitude is parameterized using a quaternion, while the local attitude error is given by a three-dimensional attitude representation. An application of the new theoretical developments is also given, which involves determining an optimal trajectory to improve the estimation accuracy of the system. A cost function is derived based upon the relative position elements of the estimator covariance. State constraints are appended to the cost function using an exponential term. Results show that minimization of this cost function yields a trajectory that improves accuracy of both the position and attitude state estimates.

I.   Introduction

Formation flight of aircraft has been an active and growing area of study in recent years. With the advent of cheaper sensors, especially micro-mechanical ones,[1] several new applications including uninhabited air vehicles (UAVs) have become mainstream. Most applications of UAVs involve military operations, some of which include reconnaissance, electronic warfare, and battle damage assessment. It is expected that thirty percent of the Air Force aircraft will be pilotless by the year 2010.[2] This growth is expected to yield a more integrated UAV arsenal capable of detection and elimination of enemy targets. Numerous civilian applications have been envisioned for the future including border interdiction, search and rescue, wild fire suppression, communications relays, law enforcement, and disaster and emergency management.[3] Cooperative UAV formations will play an important role in both military and civil applications for simultaneous coordination of resources over large areas.

Relative navigation of air vehicles flying in a formation is essential to meet mission objectives. The most common navigation mechanism for air vehicles involves the integration of Global Positioning System (GPS) signals with Inertial Measurement Units (IMUs). Both position and attitude information is possible using this type of inertial navigation system, however it requires that each vehicle must have the full GPS/IMU sensor complement. This also provides absolute information, which must be converted to relative coordinates using appropriate transformations. The relative information is often required for formation control applications and coordination.[4]

Recent investigations involve developing navigation systems without the use of GPS satellites, because the GPS signal is highly susceptible to conventional interference as well as intentional jamming and spoofing. Vision-based approaches have been developed for this purpose, which can be used for both relative and absolute navigation. These approaches have the advantage of not relying on external sensors, however they

---

*Aerospace Engineer. Email: afrl.rvsv@kirtland.af.mil. Member AIAA.

†Professor, Department of Mechanical & Aerospace Engineering. Email: johnc@eng.buffalo.edu. Associate Fellow AIAA.

American Institute of Aeronautics and Astronautics

require considerable onboard computation.[5] Reference 6 demonstrates a vision-based method of formation control and state estimation. Two approaches are used. The first incorporates an extended Kalman filter (EKF) developed in Ref. 7 with camera-based images to determine the relative states. The second approach uses image size and location to directly regulate the control algorithm. Results indicate that relative navigation is possible with a single camera.

By far the primary mechanism historically used to blend GPS measurements with IMU data has been the EKF.[8] Other implementations include an unscented Kalman filter[9] and particle filters.[10] The earliest known discussion on the use of GPS with IMUs for relative navigation occurs in Ref. 11. Relative position is propagated using a linear discrete equation, though the exact form of the state transition matrix is not provided. Increased accuracy is achieved due to the high correlation of GPS measurements between the leader and follower. These results have also been extended to vehicle platooning.[12]

In all the aforementioned papers, simplified models are used for the air vehicle dynamics. These may be adequate for a particular application, but having the full navigation equations can provide insights to the validity of using the simplified models. This derivation including a simple gravity model was first performed in Ref. 13. The relative attitude kinematics between two vehicles is well known.[14] An EKF is used for state estimation. Relative measurements involving line-of-sight (LOS) observations between the air vehicles are used, thus freeing the system from external sensors such as GPS. A minimum of three LOS observations are required for effective and accurate state estimation, even in the face of multiple initial condition errors.[13] Biased gyro and accelerometer measurements are also assumed for the follower air vehicle in order to provide full filtered position and attitude estimation.

One method for measuring LOS observations between multiple vehicles is the vision-based navigation (VISNAV) system.[15] This consists of an optical sensor combined with a specific light source (beacon) in order to achieve a selective vision. The VISNAV system is applied to the spacecraft formation flying problem in Ref. 16. State estimation is performed using an optimal observer design. Simulations show that accurate estimates of relative position and attitude are possible. An EKF is applied to the VISNAV-based relative spacecraft position and attitude estimation in Ref. 17. Automatic refueling of UAVs using a VISNAV-based system is shown in Refs. 18 and 19. Here, we focus on using the fully derived relative equations for relative air vehicle navigation.

Optimal control techniques are widely used for trajectory optimization of dynamic systems. These types of problems generally require the solution of two-point boundary value problems through use of numerical methods. An optimal control law has been designed to improve range estimation accuracy between two vehicles.[20] Motion of the system is confined to two dimensions. Components of the EKF covariance matrix are used for the cost function. This paper examines a similar cost function to determine whether the estimation accuracy of the EKF can be improved by following a specific relative trajectory.

The organization of this paper is as follows. A summary of the various coordinate frames used in this work is first provided. This is followed by a review of quaternion attitude parameters and the associated kinematics. The relative navigation equations are then developed. Next, an EKF for relative state estimation is reviewed, followed by the derivation of measurement equations. Simulation results are shown using a calibration maneuver to determine the gyro and accelerometer biases. Then an application of the relative navigation theory is shown, where a cost function is developed to minimize the position components of the state error-covariance matrix. Simulation results are also provided showing the effectiveness of the optimal control law.

II.   Reference Frames

This section summarizes the various reference frames used in the remainder of this paper, as shown in Figure 1:

- Earth-Centered-Inertial (ECI): denoted by $\{\hat{\mathbf{i}}_1, \hat{\mathbf{i}}_2, \hat{\mathbf{i}}_3\}$. The origin is at the center of the Earth, with the $\hat{\mathbf{i}}_1$ axis pointing in the direction of the vernal equinox, the $\hat{\mathbf{i}}_3$ axis pointing towards the geographic North pole, while $\hat{\mathbf{i}}_2$ completes the right-handed coordinate system. Vectors defined in this frame are identified by the letter I.

- Earth-Centered-Earth-Fixed (ECEF): denoted by $\{\hat{\mathbf{e}}_1, \hat{\mathbf{e}}_2, \hat{\mathbf{e}}_3\}$. The origin of this frame is also located at the center of the Earth. The primary difference is that this frame rotates with the Earth. The $\hat{\mathbf{e}}_3$ axis points towards the north pole and is equal to $\hat{\mathbf{i}}_3$. The $\hat{\mathbf{e}}_1$ axis is directed toward the prime
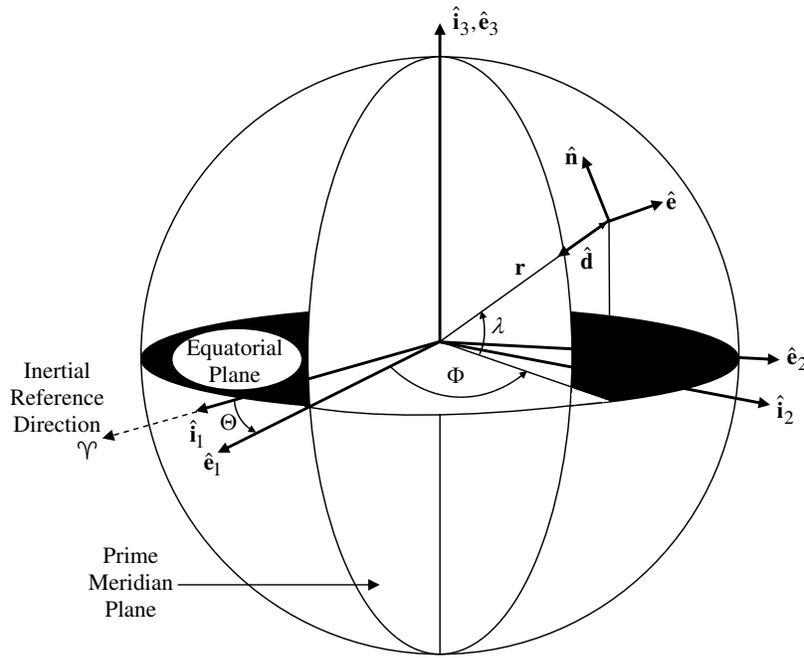
Figure 1. Definitions of Various Reference Frames

meridian, and the $\hat{\mathbf{e}}_2$ axis completes the right-handed system. The letter E signifies a vector defined with respect to this reference frame.

- North-East-Down (NED): denoted by $\{\hat{\mathbf{n}}, \hat{\mathbf{e}}, \hat{\mathbf{d}}\}$. This reference frame is commonly used for inertial navigation and is formed by fitting a tangent plane to the geodetic reference ellipse at a given point of interest.[21] The $\hat{\mathbf{n}}$ axis points North, the $\hat{\mathbf{e}}$ axis is directed East, and the $\hat{\mathbf{d}}$ axis completes the right-handed system. This reference frame is generally used for local navigation purposes. The letter N signifies a vector defined with respect to this reference frame. A thorough discussion on the conversion between the NED and ECEF frames can be found in Ref. 21.

- Body Frames: denoted by $\{\hat{\mathbf{b}}_1, \hat{\mathbf{b}}_2, \hat{\mathbf{b}}_3\}$. These are fixed to the vehicle body, rotating with it. Body frames fixed to the two air vehicles are designated leader (l) and follower (f). The letter B signifies a vector defined with respect to a generic body frame.

The convention applied in this paper is to use these letters as a superscript following the vector or matrix that is being described.

III. Attitude Kinematics

A variety of parameterizations can be used to specify attitude, including Euler angles, quaternions, and Rodrigues parameters.[22] This paper uses the quaternion, which is based on the Euler angle/axis parameterization. The quaternion is defined as $\mathbf{q} \equiv [\ \boldsymbol{\varrho}^T \quad q_4\ ]^T$ with $\boldsymbol{\varrho} = [\ q_1 \quad q_2 \quad q_3\ ]^T = \hat{\mathbf{e}} \sin(\nu/2)$, and $q_4 = \cos(\nu/2)$, where $\hat{\mathbf{e}}$ and ν are the Euler axis of rotation and rotation angle, respectively. This vector must satisfy the constraint $\mathbf{q}^T \mathbf{q} = 1$. The attitude matrix can be written as a function of the quaternion:

$$A = \Xi^T(\mathbf{q})\Psi(\mathbf{q}) \tag{1}$$

American Institute of Aeronautics and Astronautics

where

$$\Xi(\mathbf{q}) \equiv \left[\begin{array}{c} q_4 I_{3\times 3} + [\boldsymbol{\varrho}\times] \\ -\boldsymbol{\varrho}^T \end{array} \right] \tag{2a}$$

$$\Psi(\mathbf{q}) \equiv \left[\begin{array}{c} q_4 I_{3\times 3} - [\boldsymbol{\varrho}\times] \\ -\boldsymbol{\varrho}^T \end{array} \right] \tag{2b}$$

with

$$[\boldsymbol{\varrho}\times] = \left[\begin{array}{ccc} 0 & -q_3 & q_2 \\ q_3 & 0 & -q_1 \\ -q_2 & q_1 & 0 \end{array} \right] \tag{3}$$

The attitude kinematic equation is given by[23]

$$\dot{A}_I^B = -[\boldsymbol{\omega}_{B|I}^B\times]A_I^B \tag{4}$$

where $\boldsymbol{\omega}_{B|I}^B$ is the angular velocity of the body frame with respect to the inertial frame, given in body frame coordinates, and A_I^B is the attitude matrix that converts vectors from the inertial frame to the body frame.

The relative quaternion $\mathbf{q}_{f|l}$ and corresponding attitude matrix are defined by

$$\mathbf{q}_{f|l} \equiv \mathbf{q}_f \otimes \mathbf{q}_l^{-1} \tag{5a}$$

$$A_l^f \equiv A(\mathbf{q}_{f|l}) = A(\mathbf{q}_f)A^T(\mathbf{q}_l) \tag{5b}$$

which are consistent with Refs. 22 and 24. The symbol $\otimes$ denotes quaternion multiplication, given by

$$\mathbf{q}_a \otimes \mathbf{q}_b \equiv \left[\begin{array}{cc} \Psi(\mathbf{q}_a) & \mathbf{q}_a \end{array} \right] \mathbf{q}_b = \left[\begin{array}{cc} \Xi(\mathbf{q}_b) & \mathbf{q}_b \end{array} \right] \mathbf{q}_a \tag{6}$$

and $\mathbf{q}^{-1}$ is the quaternion inverse, defined by $\mathbf{q}^{-1} \equiv [-\boldsymbol{\varrho} \quad q_4]^T$.

Reference 14 shows the relative quaternion kinematics to be given by

$$\dot{\mathbf{q}}_{f|l} = \frac{1}{2}\Xi(\mathbf{q}_{f|l})\boldsymbol{\omega}_{f|l}^f \tag{7}$$

where $\boldsymbol{\omega}_{f|l}^f$ is the relative angular velocity defined as

$$\boldsymbol{\omega}_{f|l}^f \equiv \boldsymbol{\omega}_{f|E}^f - A_l^f \boldsymbol{\omega}_{l|E}^l \tag{8}$$

To reduce the computational load, a discrete form of the quaternion propagation is used. This is given by[14]

$$\mathbf{q}_{f|l_{k+1}} = \bar{\Omega}(\boldsymbol{\omega}_{f_k}^f)\bar{\Gamma}(\boldsymbol{\omega}_{l_k}^l)\mathbf{q}_{f|l_k} \tag{9}$$

where

$$\bar{\Omega}(\boldsymbol{\omega}_{f_k}^f) \equiv \left[\begin{array}{cc} \cos\left(\frac{1}{2}\|\boldsymbol{\omega}_{f_k}^f\|\Delta t\right) I_{3\times 3} - [\boldsymbol{\psi}_k\times] & \boldsymbol{\psi}_k \\ -\boldsymbol{\psi}_k^T & \cos\left(\frac{1}{2}\|\boldsymbol{\omega}_{f_k}^f\|\Delta t\right) \end{array} \right] \tag{10a}$$

$$\boldsymbol{\psi}_k \equiv \frac{\sin\left(\frac{1}{2}\|\boldsymbol{\omega}_{f_k}^f\|\Delta t\right)\boldsymbol{\omega}_{f_k}^f}{\|\boldsymbol{\omega}_{f_k}^f\|} \tag{10b}$$

$$\bar{\Gamma}(\boldsymbol{\omega}_{l_k}^l) \equiv \left[\begin{array}{cc} \cos\left(\frac{1}{2}\|\boldsymbol{\omega}_{l_k}^l\|\Delta t\right) I_{3\times 3} - [\boldsymbol{\zeta}_k\times] & -\boldsymbol{\zeta}_k \\ \boldsymbol{\zeta}_k^T & \cos\left(\frac{1}{2}\|\boldsymbol{\omega}_{l_k}^l\|\Delta t\right) \end{array} \right] \tag{10c}$$

$$\boldsymbol{\zeta}_k \equiv \frac{\sin\left(\frac{1}{2}\|\boldsymbol{\omega}_{l_k}^l\|\Delta t\right)\boldsymbol{\omega}_{l_k}^l}{\|\boldsymbol{\omega}_{l_k}^l\|} \tag{10d}$$

and Δt is the sampling interval.

IV.   Relative Position Equations

The development of the relative position equations given in Ref. 13 will be repeated here. The relative position vector is defined as

$$
\begin{aligned}
\mathbf{r}_{f|l}^f &= \mathbf{r}_{f|I}^f - A_l^f \mathbf{r}_{l|I}^l \\
&= A_I^f (\mathbf{r}_{f|I}^I - \mathbf{r}_{l|I}^I)
\end{aligned}
\tag{11}
$$

Taking two time derivatives yields

$$
\begin{aligned}
\ddot{\mathbf{r}}_{f|l}^f &= \frac{d^2}{dt^2}\left(\mathbf{r}_{f|l}^f\right) \\
&= \frac{d^2}{dt^2}\left(A_I^f\right)(\mathbf{r}_{f|I}^I - \mathbf{r}_{l|I}^I) + 2\frac{d}{dt}\left(A_I^f\right)\frac{d}{dt}(\mathbf{r}_{f|I}^I - \mathbf{r}_{l|I}^I) + A_I^f\frac{d^2}{dt^2}\left(\mathbf{r}_{f|I}^I - \mathbf{r}_{l|I}^I\right) \\
&= -\left([(\dot{\boldsymbol{\omega}}_{f|I}^f)\times] + [(\boldsymbol{\omega}_{f|I}^f)\times][(\boldsymbol{\omega}_{f|I}^f)\times]\right)A_I^f\mathbf{r}_{f|l}^I - 2[(\boldsymbol{\omega}_{f|I}^f)\times]A_I^f\dot{\mathbf{r}}_{f|l}^I + A_I^f\left(\ddot{\mathbf{r}}_{f|I}^I - \ddot{\mathbf{r}}_{l|I}^I\right) \\
&= -\dot{\boldsymbol{\omega}}_{f|I}^f \times \mathbf{r}_{f|l}^f - [(\boldsymbol{\omega}_{f|I}^f)\times][(\boldsymbol{\omega}_{f|I}^f)\times]\mathbf{r}_{f|l}^f - 2\boldsymbol{\omega}_{f|I}^f \times \dot{\mathbf{r}}_{f|l}^f + A_I^f\left(\ddot{\mathbf{r}}_{f|I}^I - \ddot{\mathbf{r}}_{l|I}^I\right)
\end{aligned}
\tag{12}
$$

The inertial accelerations of the leader and follower are given by Newton's law:

$$
\ddot{\mathbf{r}}_{l|I}^I = \mathbf{a}_l^I + \mathbf{g}_l^I
\tag{13a}
$$

$$
\ddot{\mathbf{r}}_{f|I}^I = \mathbf{a}_f^I + \mathbf{g}_f^I
\tag{13b}
$$

The gravity model in ECEF coordinates is given by

$$
\mathbf{g}^E = \frac{-\mu}{\|\mathbf{r}^E\|^3}\mathbf{r}^E
\tag{14}
$$

where $\mu = 3.986 \times 10^{14}\ m^3/(kg - s^2)$. Equation (14) provides the only nonlinear term in the relative acceleration. Equation (12) is then written as

$$
\ddot{\mathbf{r}}_{f|l}^f = -\dot{\boldsymbol{\omega}}_{f|I}^f \times \mathbf{r}_{f|l}^f - [(\boldsymbol{\omega}_{f|I}^f)\times][(\boldsymbol{\omega}_{f|I}^f)\times]\mathbf{r}_{f|l}^f - 2\boldsymbol{\omega}_{f|I}^f \times \dot{\mathbf{r}}_{f|l}^f + A_I^f\left(\mathbf{a}_f^I - \mathbf{a}_l^I\right) + A_E^f\left(\mathbf{g}_f^E - \mathbf{g}_l^E\right)
\tag{15}
$$

The acceleration measurement model is defined as

$$
\tilde{\mathbf{a}}_f^f = \mathbf{a}_f^f + \mathbf{b}_{fa} + \boldsymbol{\eta}_{fav}
\tag{16a}
$$

$$
\dot{\mathbf{b}}_{fa} = \boldsymbol{\eta}_{fau}
\tag{16b}
$$

where $\mathbf{b}_{fa}$ is the accelerometer bias, and $\boldsymbol{\eta}_{fav}$ and $\boldsymbol{\eta}_{fau}$ are zero-mean Gaussian white noise processes. Their respective spectral densities are $\sigma_{av}^2 I_{3\times3}$ and $\sigma_{au}^2 I_{3\times3}$.

The gyro measurement model has a similar form:

$$
\tilde{\boldsymbol{\omega}}_{f|I}^f = \boldsymbol{\omega}_{f|I}^f + \mathbf{b}_{fg} + \boldsymbol{\eta}_{fgv}
\tag{17a}
$$

$$
\dot{\mathbf{b}}_{fg} = \boldsymbol{\eta}_{fgu}
\tag{17b}
$$

where $\mathbf{b}_{fg}$ is the gyro bias, and $\boldsymbol{\eta}_{fgv}$ and $\boldsymbol{\eta}_{fgu}$ are zero-mean Gaussian white noise processes with spectral densities $\sigma_{gv}^2 I_{3\times3}$ and $\sigma_{gu}^2 I_{3\times3}$. See the appendix of Ref. 25 for a more detailed discussion on the gyro bias model.

V.   Extended Kalman Filter Equations

The states of interest in this EKF are relative attitude, relative position, relative velocity, and biases on the inertial acceleration and angular velocity measurements:

$$
\mathbf{x} = \begin{bmatrix} \mathbf{q}_{f|l}^T & (\mathbf{r}_{f|l}^f)^T & (\dot{\mathbf{r}}_{f|l}^f)^T & \mathbf{b}_{fg}^T & \mathbf{b}_{fa}^T \end{bmatrix}^T
\tag{18}
$$

American Institute of Aeronautics and Astronautics

The following estimate equations are based on the truth equations of the prior sections:

$$\dot{\hat{\mathbf{q}}}_{f|l} = \frac{1}{2}\Xi(\hat{\mathbf{q}}_{f|l})\hat{\boldsymbol{\omega}}^f_{f|l} \tag{19a}$$

$$\ddot{\hat{\mathbf{r}}}^f_{f|l} = -\dot{\hat{\boldsymbol{\omega}}}^f_{f|I} \times \hat{\mathbf{r}}^f_{f|l} - [(\hat{\boldsymbol{\omega}}^f_{f|I})\times][(\hat{\boldsymbol{\omega}}^f_{f|I})\times]\hat{\mathbf{r}}^f_{f|l} - 2\hat{\boldsymbol{\omega}}^f_{f|I} \times \dot{\hat{\mathbf{r}}}^f_{f|l} + \hat{A}^f_I\left(\hat{\mathbf{a}}^I_f - \mathbf{a}^I_l\right) + \hat{A}^f_E\left(\hat{\mathbf{g}}^E_f - \mathbf{g}^E_l\right) \tag{19b}$$

$$\hat{\mathbf{a}}^f_f = \tilde{\mathbf{a}}^f_f - \hat{\mathbf{b}}_{fa} \tag{19c}$$

$$\hat{\mathbf{g}}^E_f = \frac{-\mu}{\|\hat{\mathbf{r}}^E_{f|E}\|^3}\hat{\mathbf{r}}^E_{f|E} \tag{19d}$$

$$\hat{\boldsymbol{\omega}}^f_{f|I} = \tilde{\boldsymbol{\omega}}^f_{f|I} - \hat{\mathbf{b}}_{fg} \tag{19e}$$

$$\dot{\hat{\mathbf{b}}}_{fa} = \mathbf{0} \tag{19f}$$

$$\dot{\hat{\mathbf{b}}}_{fg} = \mathbf{0} \tag{19g}$$

The state-error vector is given as

$$\Delta\mathbf{x} = \begin{bmatrix} \boldsymbol{\delta\alpha}^T_{f|l} & (\Delta\mathbf{r}^f_{f|l})^T & (\Delta\dot{\mathbf{r}}^f_{f|l})^T & \Delta\mathbf{b}^T_{fg} & \Delta\mathbf{b}^T_{fa} \end{bmatrix}^T \tag{20}$$

The first term is defined by

$$\boldsymbol{\delta\alpha}_{f|l} = 2\boldsymbol{\delta\varrho}_{f|l} \tag{21a}$$

$$\boldsymbol{\delta\mathbf{q}}_{f|l} = \mathbf{q}_{f|l} \otimes \hat{\mathbf{q}}^{-1}_{f|l} \tag{21b}$$

where $\boldsymbol{\delta\alpha}_{f|l}$ corresponds to a vector of half-error angles for any small roll, pitch and yaw sequence, and $\boldsymbol{\delta\varrho}_{f|l}$ denotes the first three components of the four component vector $\boldsymbol{\delta\mathbf{q}}_{f|l}$. The usual EKF assumption that the estimate is close, to within first-order dominate terms, to the truth is applied. For this case, the fourth error-component is approximately one and its derivative is near zero.[24] The remaining state-error terms are defined generically as $\Delta\mathbf{y} = \mathbf{y} - \hat{\mathbf{y}}$, while the process noise vector consists of the four Gaussian noise terms from the measurement equations:

$$\mathbf{w} = \begin{bmatrix} \boldsymbol{\eta}^T_{fgv} & \boldsymbol{\eta}^T_{fgu} & \boldsymbol{\eta}^T_{fav} & \boldsymbol{\eta}^T_{fau} \end{bmatrix}^T \tag{22}$$

The next step is to determine time derivatives of the error states. The equation for $\boldsymbol{\delta\dot{\alpha}}_{f|l}$ is given in Ref. 26 as

$$\boldsymbol{\delta\dot{\alpha}}_{f|l} = -[(\hat{\boldsymbol{\omega}}^f_{f|l})\times]\boldsymbol{\delta\alpha}_{f|l} + \boldsymbol{\delta\omega}^f_{f|l} \tag{23}$$

where

$$\boldsymbol{\delta\omega}^f_{f|l} = \boldsymbol{\omega}^f_{f|l} - \hat{\boldsymbol{\omega}}^f_{f|l} \tag{24}$$

Based upon the definitions in Eqs. (8) and (17a), along with the approximation

$$A^f_l = (I_{3\times3} - [(\boldsymbol{\delta\alpha}_{f|l})\times])\hat{A}^f_l \tag{25}$$

Eq. (24) becomes

$$\boldsymbol{\delta\omega}^f_{f|l} = -\Delta\mathbf{b}_{fg} - \boldsymbol{\eta}_{fgv} - [(\hat{A}^f_l\boldsymbol{\omega}^l_{l|I})\times]\boldsymbol{\delta\alpha}_{f|l} \tag{26}$$

Equation (23) then simplifies to

$$\boldsymbol{\delta\dot{\alpha}}_{f|l} = -[(\hat{\boldsymbol{\omega}}^f_{f|I})\times]\boldsymbol{\delta\alpha}_{f|l} - \Delta\mathbf{b}_{fg} - \boldsymbol{\eta}_{fgv} \tag{27}$$

The time derivative of the position error-state vector is simply equal to the velocity error state vector:

$$\frac{d}{dt}(\Delta\mathbf{r}^f_{f|l}) = \Delta\dot{\mathbf{r}}^f_{f|l} \tag{28}$$

The time derivative of the velocity vector is more complicated. To keep this paper concise, the algebraic derivation of this equation will be omitted. The final result makes use of several of the relations already mentioned in this paper, along with Euler's equation[23]

$$\dot{\boldsymbol{\omega}}^f_{f|I} = J^{-1}_f\left(\mathbf{u}_f - [(\boldsymbol{\omega}^f_{f|I})\times]J_f\boldsymbol{\omega}^f_{f|I}\right) \tag{29}$$

where J_f is the inertia matrix of the follower and $\mathbf{u}_f$ is the applied torque. An expansion of the gravity model in Eq. (14) is also required:

$$\mathbf{g}_f^E = \hat{\mathbf{g}}_f^E + \frac{\partial \mathbf{g}_f^E}{\partial \Delta \mathbf{r}_{f|l}^f} \Delta \mathbf{r}_{f|l}^f + \frac{\partial \mathbf{g}_f^E}{\partial \boldsymbol{\delta \alpha}_{f|l}} \boldsymbol{\delta \alpha}_{f|l} \tag{30}$$

where

$$
\frac{\partial \mathbf{g}_f^E}{\partial \Delta \mathbf{r}_{f|l}^f} = -\mu \hat{A}_f^E \| \mathbf{r}_{l|I}^E + \hat{A}_f^E \hat{\mathbf{r}}_{f|l}^f \|^{-3}
$$
$$
+ 3\mu \left(\mathbf{r}_{l|I}^E + \hat{A}_f^E \hat{\mathbf{r}}_{f|l}^f \right) \left(\mathbf{r}_{l|I}^E + \hat{A}_f^E \hat{\mathbf{r}}_{f|l}^f \right)^T \| \mathbf{r}_{l|I}^E + \hat{A}_f^E \hat{\mathbf{r}}_{f|l}^f \|^{-5} \tag{31}
$$

$$
\frac{\partial \mathbf{g}_f^E}{\partial \boldsymbol{\delta \alpha}_{f|l}} = -\mu \hat{A}_f^E [(\hat{\mathbf{r}}_{f|l}^f) \times] \| \mathbf{r}_{l|I}^E + \hat{A}_f^E \hat{\mathbf{r}}_{f|l}^f \|^{-3}
$$
$$
+ 3\mu \left(\mathbf{r}_{l|I}^E + \hat{A}_f^E \hat{\mathbf{r}}_{f|l}^f \right) \left(\mathbf{r}_{l|I}^E + \hat{A}_f^E \hat{\mathbf{r}}_{f|l}^f \right)^T \hat{A}_E^f [(\hat{\mathbf{r}}_{f|l}^f) \times] \| \mathbf{r}_{l|I}^E + \hat{A}_E^f \hat{\mathbf{r}}_{f|l}^f \|^{-5} \tag{32}
$$

Using the above relations, the velocity error-dynamics equation is written as

$$
\frac{d}{dt} \Delta \dot{\mathbf{r}}_{f|l}^f = F_{3-1} \boldsymbol{\delta \alpha}_{f|l} + F_{3-2} \Delta \mathbf{r}_{f|l}^f + F_{3-3} \Delta \dot{\mathbf{r}}_{f|l}^f + F_{3-4} \Delta \mathbf{b}_{fg}
$$
$$
+ F_{3-5} \Delta \mathbf{b}_{fa} + G_{3-1} \boldsymbol{\eta}_{fgv} + G_{3-3} \boldsymbol{\eta}_{fav} \tag{33}
$$

where

$$
F_{3-1} = - [(\hat{A}_l^f \mathbf{a}_l^l) \times] + [(\hat{A}_E^f (\hat{\mathbf{g}}_f^E - \mathbf{g}_l^E)) \times] - \mu \hat{A}_E^f \left\{ \hat{A}_f^E [(\hat{\mathbf{r}}_{f|l}^f) \times] \| \mathbf{r}_{l|I}^E + \hat{A}_f^E \hat{\mathbf{r}}_{f|l}^f \|^{-3} \right.
$$
$$
\left. - 3 \left(\mathbf{r}_{l|I}^E + \hat{A}_f^E \hat{\mathbf{r}}_{f|l}^f \right) \left(\mathbf{r}_{l|I}^E + \hat{A}_f^E \hat{\mathbf{r}}_{f|l}^f \right)^T \hat{A}_f^E [(\hat{\mathbf{r}}_{f|l}^f) \times] \| \mathbf{r}_{l|I}^E + \hat{A}_f^E \hat{\mathbf{r}}_{f|l}^f \|^{-5} \right\} \tag{34a}
$$

$$
F_{3-2} = - [(\hat{\boldsymbol{\omega}}_{f|I}^f) \times][(\hat{\boldsymbol{\omega}}_{f|I}^f) \times] - [(\dot{\hat{\boldsymbol{\omega}}}_{f|I}^f) \times] - \mu \hat{A}_E^f \left\{ \hat{A}_f^E \| \mathbf{r}_{l|I}^E + \hat{A}_f^E \hat{\mathbf{r}}_{f|l}^f \|^{-3} \right.
$$
$$
\left. - 3 \left(\mathbf{r}_{l|I}^E + \hat{A}_f^E \hat{\mathbf{r}}_{f|l}^f \right) \left((\mathbf{r}_{l|I}^E)^T + (\hat{A}_f^E \hat{\mathbf{r}}_{f|l}^f)^T \right) \| \mathbf{r}_{l|I}^E + \hat{A}_f^E \hat{\mathbf{r}}_{f|l}^f \|^{-5} \right\} \tag{34b}
$$

$$
F_{3-3} = -2[(\hat{\boldsymbol{\omega}}_{f|I}^f) \times] \tag{34c}
$$

$$
F_{3-4} = - [(\hat{\mathbf{r}}_{f|l}^f) \times] J_f^{-1} \left\{ [(J_f \hat{\boldsymbol{\omega}}_{f|I}^f) \times] - [(\hat{\boldsymbol{\omega}}_{f|I}^f) \times] J_f \right\} - 2[(\dot{\hat{\mathbf{r}}}_{f|l}^f) \times]
$$
$$
- \left([(\hat{\boldsymbol{\omega}}_{f|I}^f \times \hat{\mathbf{r}}_{f|l}^f) \times] + [(\hat{\boldsymbol{\omega}}_{f|I}^f) \times][(\hat{\mathbf{r}}_{f|l}^f) \times] \right) \tag{34d}
$$

$$
F_{3-5} = -I_3 \tag{34e}
$$

$$
G_{3-1} = - [(\hat{\mathbf{r}}_{f|l}^f) \times] J_f^{-1} \left\{ [(J_f \hat{\boldsymbol{\omega}}_{f|I}^f) \times] - [(\hat{\boldsymbol{\omega}}_{f|I}^f) \times] J_f \right\} - 2[(\dot{\hat{\mathbf{r}}}_{f|l}^f) \times]
$$
$$
- \left([(\hat{\boldsymbol{\omega}}_{f|I}^f \times \hat{\mathbf{r}}_{f|l}^f) \times] + [(\hat{\boldsymbol{\omega}}_{f|I}^f) \times][(\hat{\mathbf{r}}_{f|l}^f) \times] \right) \tag{34f}
$$

$$
G_{3-3} = -I_3 \tag{34g}
$$

Lastly, the time derivatives of the bias states are found by using Eqs. (16b) through (17b):

$$
\Delta \dot{\mathbf{b}}_{fa} = \boldsymbol{\eta}_{fau} \tag{35a}
$$
$$
\Delta \dot{\mathbf{b}}_{fg} = \boldsymbol{\eta}_{fgu} \tag{35b}
$$

The overall error dynamics are governed by the equation

$$
\Delta \dot{\mathbf{x}} = F \Delta \mathbf{x} + G \mathbf{w} \tag{36}
$$

where the F and G matrices are given by

$$F = \begin{bmatrix} -[(\hat{\boldsymbol{\omega}}^f_{f|I})\times] & 0_{3\times3} & 0_{3\times3} & -I_{3\times3} & 0_{3\times3} \\ 0_{3\times3} & 0_{3\times3} & I_{3\times3} & 0_{3\times3} & 0_{3\times3} \\ F_{3-1} & F_{3-2} & F_{3-3} & F_{3-4} & F_{3-5} \\ 0_{3\times3} & 0_{3\times3} & 0_{3\times3} & 0_{3\times3} & 0_{3\times3} \\ 0_{3\times3} & 0_{3\times3} & 0_{3\times3} & 0_{3\times3} & 0_{3\times3} \end{bmatrix} \tag{37}$$

$$G = \begin{bmatrix} -I_{3\times3} & 0_{3\times3} & 0_{3\times3} & 0_{3\times3} \\ 0_{3\times3} & 0_{3\times3} & 0_{3\times3} & 0_{3\times3} \\ G_{3-1} & 0_{3\times3} & G_{3-3} & 0_{3\times3} \\ 0_{3\times3} & I_{3\times3} & 0_{3\times3} & 0_{3\times3} \\ 0_{3\times3} & 0_{3\times3} & 0_{3\times3} & I_{3\times3} \end{bmatrix} \tag{38}$$

The process noise covariance matrix used in the EKF is

$$Q = \begin{bmatrix} \sigma^2_{fgv}I_{3\times3} & 0_{3\times3} & 0_{3\times3} & 0_{3\times3} \\ 0_{3\times3} & \sigma^2_{fgu}I_{3\times3} & 0_{3\times3} & 0_{3\times3} \\ 0_{3\times3} & 0_{3\times3} & \sigma^2_{fav}I_{3\times3} & 0_{3\times3} \\ 0_{3\times3} & 0_{3\times3} & 0_{3\times3} & \sigma^2_{fau}I_{3\times3} \end{bmatrix} \tag{39}$$

A discrete propagation is used for the covariance matrix in order to reduce the computational load:

$$P^-_{k+1} = \Phi_k P^+_k \Phi^T_k + \mathcal{Q}_k \tag{40}$$

where Φ_k is the state transition matrix and $\mathcal{Q}_k$ is the covariance matrix. Reference 27 gives a numerical solution for these matrices. The first step is to set up the following $2n$ by $2n$ matrix:

$$\mathcal{A} = \begin{bmatrix} -F & GQG^T \\ 0_{n\times n} & F^T \end{bmatrix} \Delta t \tag{41}$$

The matrix exponential is then calculated:

$$\mathcal{B} = e^{\mathcal{A}} = \begin{bmatrix} \mathcal{B}_{11} & \mathcal{B}_{12} \\ 0_{n\times n} & \mathcal{B}_{22} \end{bmatrix} = \begin{bmatrix} \mathcal{B}_{11} & \Phi^{-1}_k \mathcal{Q}_k \\ 0_{n\times n} & \Phi^T_k \end{bmatrix} \tag{42}$$

The state transition and covariance matrices are then given as

$$\Phi_k = \mathcal{B}^T_{22} \tag{43a}$$
$$\mathcal{Q}_k = \Phi_k \mathcal{B}_{12} \tag{43b}$$

Note that Eq. (41) is only valid for constant system and covariance matrices. However, for small Δt it is a good approximation of the actual discrete-time matrices that are time varying.

A. Measurement Equations

The measurements used in this filter consist of the relative LOS observations between the two air vehicles. A schematic of this system is shown in Fig. 2. Beacons are located on the follower at coordinates specified in the follower reference frame by (X_i, Y_i, Z_i). The relations between image space measurements of the sensor (α_i, β_i) to the object space, using a focal plane detector to detect the beacon light, are given by[28]

$$\alpha_i = -f\frac{A^f_{l_{11}}(X_i + x) + A^f_{l_{21}}(Y_i + y) + A^f_{l_{31}}(Z_i + z)}{A^f_{l_{13}}(X_i + x) + A^f_{l_{23}}(Y_i + y) + A^f_{l_{33}}(Z_i + z)} \tag{44a}$$

$$\beta_i = -f\frac{A^f_{l_{12}}(X_i + x) + A^f_{l_{22}}(Y_i + y) + A^f_{l_{32}}(Z_i + z)}{A^f_{l_{13}}(X_i + x) + A^f_{l_{23}}(Y_i + y) + A^f_{l_{33}}(Z_i + z)} \tag{44b}$$

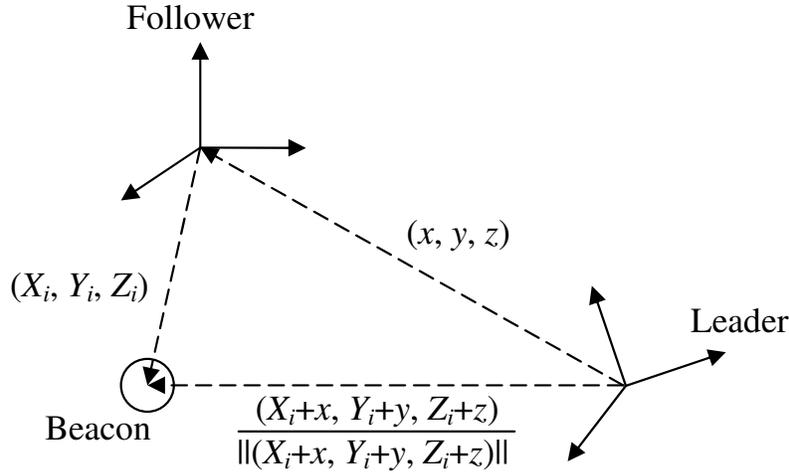American Institute of Aeronautics and Astronautics

Figure 2. Vision Based Navigation System

where f is the focal length, and the $A^f_{l_{ij}}$ are components of the attitude matrix A^f_l, which transforms vectors from the leader frame to the follower frame. Since observations can be given as α_i/f and β_i/f, the focal length is set equal to one in order to simplify the math. The (x, y, z) coordinates are the components of the vector $\mathbf{r}^f_{f|l}$.

Consider a measurement vector denoted by

$$\tilde{\boldsymbol{\gamma}}_i = \boldsymbol{\gamma}_i + \mathbf{v} \tag{45a}$$

$$\boldsymbol{\gamma}_i \equiv \begin{bmatrix} \alpha_i \\ \beta_i \end{bmatrix} \tag{45b}$$

A frequently used covariance of $\mathbf{v}$ is given by Ref. 29 as

$$R_i^{\text{FOCAL}} = \frac{\sigma^2}{1 + d(\alpha_i^2 + \beta_i^2)} \begin{bmatrix} (1 + d\alpha_i^2)^2 & (d\alpha_i\beta_i)^2 \\ (d\alpha_i\beta_i)^2 & (1 + d\beta_i^2)^2 \end{bmatrix} \tag{46}$$

where d is on the order of 1 and σ is assumed to be known. Note that the components of this covariance matrix will increase as the image space coordinates increase. This demonstrates that errors will increase as the observation moves away from the boresight. Reference 29 also states that for practical purposes, the estimated values of α_i and β_i must be used in place of the true quantities. This only leads to second-order error effects.

The problem with using Eq. (45a) as the measurement vector is that the definitions of α_i and β_i in Eq. (44) are highly nonlinear in both the position and attitude components. A simpler observation vector is given in unit vector form as

$$\mathbf{b}_i = (A^f_l)^T \mathbf{r}_i \tag{47a}$$

$$\mathbf{r}_i \equiv \frac{\mathbf{R}_i + \mathbf{r}^f_{f|l}}{\|\mathbf{R}_i + \mathbf{r}^f_{f|l}\|} \tag{47b}$$

where $\mathbf{R}_i = \begin{bmatrix} X_i & Y_i & Z_i \end{bmatrix}^T$, $\mathbf{r}^f_{f|l} \equiv \begin{bmatrix} x & y & z \end{bmatrix}^T$, and for a sensor facing in the positive Z direction,

$$\mathbf{b}_i = \frac{1}{\sqrt{1 + \alpha_i^2 + \beta_i^2}} \begin{bmatrix} -\alpha_i \\ -\beta_i \\ 1 \end{bmatrix} \tag{48}$$

American Institute of Aeronautics and Astronautics

Similar equations for the positive X and Y directions are found by rotating the elements of the vector in a cyclic manner. Sensors facing in the negative direction use the same equations multiplied by -1.

The QUEST measurement model shown in Ref. 30 works well for small field-of-view sensors, but may produce significant errors for larger field of views, such as the VISNAV sensor. A new covariance model is developed in Ref. 31 that provides better accuracy than the QUEST model for this case. It is based upon a first-order Taylor series expansion of the unit vector observation. The primary assumption is that the measurement noise is small compared to the signal. The new covariance is defined as

$$R_i^{\text{NEW}} = J_i R_i^{\text{FOCAL}} J_i^T \tag{49}$$

where J_i is the Jacobian of Eq. (48) and is given by

$$J_i \equiv \frac{\partial \mathbf{b}_i}{\partial \boldsymbol{\gamma}_i} = \frac{1}{\sqrt{1 + \alpha_i^2 + \beta_i^2}} \begin{bmatrix} -1 & 0 \\ 0 & -1 \\ 0 & 0 \end{bmatrix} - \frac{1}{1 + \alpha_i^2 + \beta_i^2} \mathbf{b}_i \begin{bmatrix} \alpha_i & \beta_i \end{bmatrix} \tag{50}$$

Appropriate modifications to the Jacobian must be made for sensors facing along the other axes. It should be noted that R_i^{NEW} is also a singular matrix. This issue must be overcome before the covariance can be used within the EKF framework. A rank-one update approach is shown effective to overcome this difficulty, as shown in Ref. 31. The basic idea is to add an additional term $c_i \mathbf{b}_i \mathbf{b}_i^T$ $(c_i > 0)$ to the measurement covariance matrix to ensure that the new covariance matrix is nonsingular and does not change the overall result in the EKF. This is mathematically written as

$$\mathcal{R}_i^{\text{NEW}} = R_i^{\text{NEW}} + c_i \mathbf{b}_i \mathbf{b}_i^T \tag{51}$$

The coefficient c_i is recommended to be given by

$$c_i = \frac{1}{2} \text{trace}(R_i^{\text{NEW}}) \tag{52}$$

where trace is the mathematical function denoting trace of a matrix.

The next step is to determine the partial derivative of the measurement vector with respect to the state vector in order to form the H matrix of the filter. Using Eq. (25), Eq. (47a) becomes

$$\begin{aligned} \mathbf{b}_i &= (\hat{A}_l^f)^T (I_{3\times3} + [(\boldsymbol{\delta\alpha}_{f|l})\times]) \mathbf{r}_i \\ &= (\hat{A}_l^f)^T \mathbf{r}_i + (\hat{A}_l^f)^T [(\boldsymbol{\delta\alpha}_{f|l})\times] \mathbf{r}_i \\ &= (\hat{A}_l^f)^T \mathbf{r}_i - (\hat{A}_l^f)^T [(\mathbf{r}_i)\times] \boldsymbol{\delta\alpha}_{f|l} \end{aligned} \tag{53}$$

The partial derivative with respect to the attitude states is simply given by

$$\frac{\partial \mathbf{b}_i}{\partial \boldsymbol{\delta\alpha}_l^f} = -(\hat{A}_l^f)^T [(\mathbf{r}_i)\times] \tag{54}$$

The partial derivative with respect to the position vector is more complicated, and given by Ref. 17:

$$\begin{aligned} \frac{\partial \mathbf{b}_i}{\partial \mathbf{r}_{f|l}^f} &= (A_l^f)^T \frac{\partial \mathbf{r}_i}{\partial \mathbf{r}_{f|l}^f} \\ &= (A_l^f)^T \frac{1}{\|\mathbf{R}_i + \mathbf{r}_{f|l}^f\|} \left(I_{3\times3} - \frac{1}{\|\mathbf{R}_i + \mathbf{r}_{f|l}^f\|^2} (\mathbf{R}_i + \mathbf{r}_{f|l}^f)(\mathbf{R}_i + \mathbf{r}_{f|l}^f)^T \right) \end{aligned} \tag{55}$$

The overall sensitivity matrix is then given as

$$H_i = \begin{bmatrix} \dfrac{\partial \mathbf{b}_i}{\partial \boldsymbol{\delta\alpha}_l^f} & \dfrac{\partial \mathbf{b}_i}{\partial \mathbf{r}_{f|l}^f} & 0_{3\times3} & 0_{3\times3} & 0_{3\times3} \end{bmatrix} \tag{56}$$

The complete EKF is summarized in Table 1, where R_k is the block-diagonal matrix made up of all the individual $\mathcal{R}_{i_k}^{\text{NEW}}$ matrices, $\tilde{\mathbf{y}}_k \equiv [\tilde{\mathbf{b}}_{1_k}^T \cdots \tilde{\mathbf{b}}_{N_k}^T]^T$ and $\hat{\mathbf{y}}_k^- \equiv [\hat{\mathbf{b}}_{1_k}^{-T} \cdots \hat{\mathbf{b}}_{N_k}^{-T}]^T$, where N is the total number of LOS observations at time t_k. Detailed simulation results can be seen in Ref. 13. The filter is shown robust to initial condition errors in all states.[13] From the state error plots, a minimum of three beacons is seen to be necessary for continuous convergence of all covariance bounds. Also, relative gravity terms are shown to be important for the case of using only one beacon to update the states. Therefore, these terms should not be ignored in general.

Table 1. Summary of Extended Kalman Filter for Relative Inertial Navigation

Initialize	$\hat{\mathbf{q}}_{fl}(t_0) = \mathbf{q}_{f\|l0}$ $\hat{\mathbf{r}}_{f\|l}^{f}(t_0) = \mathbf{r}_{f\|l0}^{f}$ $\hat{\mathbf{v}}_{f\|l}^{f}(t_0) = \mathbf{v}_{f\|l0}^{f}$ $\boldsymbol{\beta}_{fg}(t_0) = \boldsymbol{\beta}_{fg0}$ $\boldsymbol{\beta}_{fa}(t_0) = \boldsymbol{\beta}_{fa0}$ $P(t_0) = P_0$
Gain	$K_k = P_k^- H_k^T(\hat{\mathbf{x}}_k^-)[H_k(\hat{\mathbf{x}}_k^-)P_k^- H_k^T(\hat{\mathbf{x}}_k^-) + R_k]^{-1}$ $H_k(\hat{\mathbf{x}}_k^-) = \left[\begin{array}{ccccc} \frac{\partial \mathbf{b}_i}{\partial \boldsymbol{\delta\alpha}_l^f} & \frac{\partial \mathbf{b}_i}{\partial \mathbf{r}_{f\|l}^f} & 0_{3\times3} & 0_{3\times3} & 0_{3\times3} \end{array} \right]\Big\|_{t_k}$
Update	$P_k^+ = [I - K_k H_k(\hat{\mathbf{x}}^-)]P_k^-$ $\Delta\hat{\hat{\mathbf{x}}}_k^+ = K_k[\tilde{\mathbf{y}}_k - \hat{\mathbf{y}}_k^-]$ $\Delta\hat{\hat{\mathbf{x}}}_k^+ \equiv \left[\begin{array}{ccccc} \boldsymbol{\delta\alpha}_{f\|l_k}^{+T} & \Delta\mathbf{r}_{f\|l_k}^{f} & \Delta\mathbf{v}_{f\|l_k}^{f} & \Delta\boldsymbol{\beta}_{fg_k}^{+T} & \Delta\boldsymbol{\beta}_{fa_k}^{+T} \end{array} \right]$ $\hat{\mathbf{q}}_{f\|l_k}^+ = \hat{\mathbf{q}}_{f\|l_k}^- + \frac{1}{2}\Xi(\hat{\mathbf{q}}_{f\|l_k}^-)\boldsymbol{\delta\alpha}_{f\|l_k}$ $\hat{\mathbf{q}}_{f\|l_k}^+ = \frac{\hat{\mathbf{q}}_{f\|l_k}^+}{\|\hat{\mathbf{q}}_{f\|l_k}^+\|}$ $\hat{\mathbf{r}}_{f\|l_k}^{f+} = \hat{\mathbf{r}}_{f\|l_k}^{f-} + \Delta\mathbf{r}_{f\|l_k}^{f}$ $\hat{\mathbf{v}}_{f\|l_k}^{f+} = \hat{\mathbf{v}}_{f\|l_k}^{f-} + \Delta\mathbf{v}_{f\|l_k}^{f}$ $\hat{\boldsymbol{\beta}}_{fg_k}^+ = \hat{\boldsymbol{\beta}}_{fg_k}^- + \Delta\hat{\boldsymbol{\beta}}_{fg_k}^+$ $\hat{\boldsymbol{\beta}}_{fa_k}^+ = \hat{\boldsymbol{\beta}}_{fa_k}^- + \Delta\hat{\boldsymbol{\beta}}_{fa_k}^+$
Propagation	$\hat{\mathbf{a}}_{f_k}^{f+} = \tilde{\mathbf{a}}_{f_k}^{f} - \hat{\boldsymbol{\beta}}_{fa_k}^+$ $\hat{\boldsymbol{\omega}}_{f\|I_k}^{f+} = \tilde{\boldsymbol{\omega}}_{f\|I_k}^{f} - \hat{\boldsymbol{\beta}}_{fg_k}^+$ $\hat{\mathbf{q}}_{f\|l_{k+1}}^- = \bar{\Omega}(\hat{\boldsymbol{\omega}}_{f\|I_k}^{f+})\bar{\Gamma}(\boldsymbol{\omega}_{l\|I_k}^{l+})\hat{\mathbf{q}}_{f\|l_k}^+$ $P_{k+1}^- = \Phi_k P_k^+ \Phi_k^T + \mathcal{Q}_k$ $\ddot{\mathbf{r}}_{f\|l}^{f} = -\dot{\hat{\boldsymbol{\omega}}}_{f\|I}^{f} \times \hat{\mathbf{r}}_{f\|l}^{f} - [(\hat{\boldsymbol{\omega}}_{f\|I}^{f})\times][(\hat{\boldsymbol{\omega}}_{f\|I}^{f})\times]\hat{\mathbf{r}}_{f\|l}^{f} - 2\hat{\boldsymbol{\omega}}_{f\|I}^{f} \times \dot{\hat{\mathbf{r}}}_{f\|l}^{f}$ $\qquad + \hat{\mathbf{a}}_f^f - \hat{A}_l^f \mathbf{a}_l^l + \hat{A}_E^f\left(\hat{\mathbf{g}}_f^E - \mathbf{g}_l^E\right)$ $\hat{\mathbf{g}}_f^E = \frac{-\mu}{\|\hat{\mathbf{r}}_{f\|E}^E\|^3}\hat{\mathbf{r}}_{f\|E}^E$

B. Calibration Maneuver Simulation Results

In this section simulations results are shown that involve a calibration maneuver designed to estimate the gyro and accelerometer biases while also estimating the position and attitude. Leader states are assumed known aboard the follower. Realistically, there will be some delay between filtering of measurements onboard the leader and receipt of the state estimates on the follower. For a relative distance of 1 km, it will take approximately 10^{-5} seconds for a communication signal to be transmitted between the two vehicles. Adding in the computational effort of data processing and signal transmission, it is assumed that the overall lag will still be significantly smaller than filter update period. With that being the case, the received leader states can be propagated forward over the lag interval without significant loss in accuracy.

Trajectories for all simulations are given in the NED frame for a location of interest starting at a latitude

American Institute of Aeronautics and Astronautics

Table 2. List of Beacon Locations

Beacon Number (i)	X_i	Y_i	Z_i
1	0 m	7 m	0 m
2	−3.75 m	2.25 m	−1.5 m
3	3.75 m	0 m	0 m
4	1.5 m	0 m	0 m
5	0 m	−7 m	0 m
6	3.75 m	−2.25 m	1.5 m
7	−3.75 m	0 m	0 m
8	−1.5 m	0 m	0 m

Table 3. Noise Parameters

Gyro Noise		Accelerometer Noise		VISNAV Noise
$\sigma_{gv} = 8.7266 \times 10^{-7} \frac{\text{rad}}{\text{s}^{1/2}}$		$\sigma_{av} = 1.5 \times 10^{-5} \frac{\text{m}}{\text{s}^{3/2}}$		$\sigma_m = 350\ \mu\text{rad} = 72.2$ arc-s
$\sigma_{gu} = 2.15 \times 10^{-8} \frac{\text{rad}}{\text{s}^{3/2}}$		$\sigma_{au} = 6.0 \times 10^{-5} \frac{\text{m}}{\text{s}^{5/2}}$		

of 38 degrees, longitude of -77 degrees and zero height. The leader trajectory is given by

$$\mathbf{r}_{l|N}^{N} = \begin{bmatrix} 50t \\ 1000\sin(0.005t) \\ -10t \end{bmatrix} \text{ meters} \tag{57}$$

In practice, following the given trajectory will result in minor changes in attitude. Here it is assumed that the attitude with respect to the NED reference frame remains constant, which allows for a fairly realistic scenario that doesn't require a control system with vehicle dynamics. For an actual system, this will be heavily tied to the aerodynamics of the chosen air vehicle, which is beyond the scope of the current paper. Eight beacons whose position are shown in Table 2 will be used. Another assumption is made that the beacons will always be visible to the focal plane arrays onboard the leader. This will generally not happen in practice since parts of the air vehicle itself will block the lines of sight. Since that depends upon the specific air vehicle being used, this factor will not be simulated here. The subsequent results should be thought of as having enough beacons on the follower such that eight will always have clear lines of sight.

The relative position trajectory for this maneuver will be given by

$$\mathbf{r}_{f|l}^{N} = \begin{bmatrix} 75\cos(\omega_r t) \\ 75\sin(\omega_r t) \\ 30 \end{bmatrix} \text{ meters} \tag{58}$$

where $\omega_r = 2\pi/3600$ rad/s. The rotational rate of the follower is given by $\boldsymbol{\omega}_{f|N}^{N} = \begin{bmatrix} 0 & 0 & \omega_r \end{bmatrix}^T$. This maneuver should be slow enough such that it can be followed by most available air vehicle. Gyro, accelerometer and VISNAV measurements are sampled at 10 Hz using noise parameters given in Table 3. The initial gyro and accelerometer biases are given by $\boldsymbol{\beta}_{fg} = [0.8\ -0.75\ 0.6]^T$ deg/hr and $\boldsymbol{\beta}_{fa} = [-0.002\ 0.0375\ -0.004]^T$ m/s^2. Both the accelerometer and gyro biases are initially assumed to be zero in the EKF. The initial covariance matrix P_0 is diagonal. The attitude components of the covariance are initialized to a 3σ bound of 5 deg. The position and velocity parts have 3σ bounds of 20 m and 0.5 m/s, respectively. The accelerometer and gyro bias components have 3σ bounds 1 deg/hr and 0.1 m/s^2, respectively.

Figures 3 and 4 show the estimation errors for the calibration maneuver. All plots show the average of errors over 100 Monte Carlo runs. Estimates of all states can be seen to converge within their respective theoretical covariance bounds. Position errors are contained within 3σ bounds of 10 cm, while the attitude
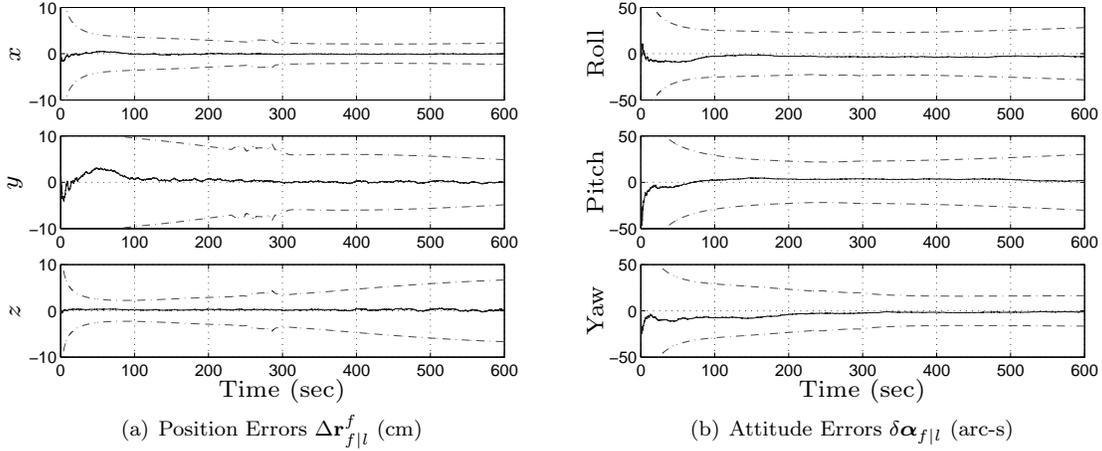
American Institute of Aeronautics and Astronautics

(a) Position Errors $\Delta \mathbf{r}_{f|l}^f$ (cm)

(b) Attitude Errors $\delta \boldsymbol{\alpha}_{f|l}$ (arc-s)

Figure 3. Relative Position and Attitude Errors

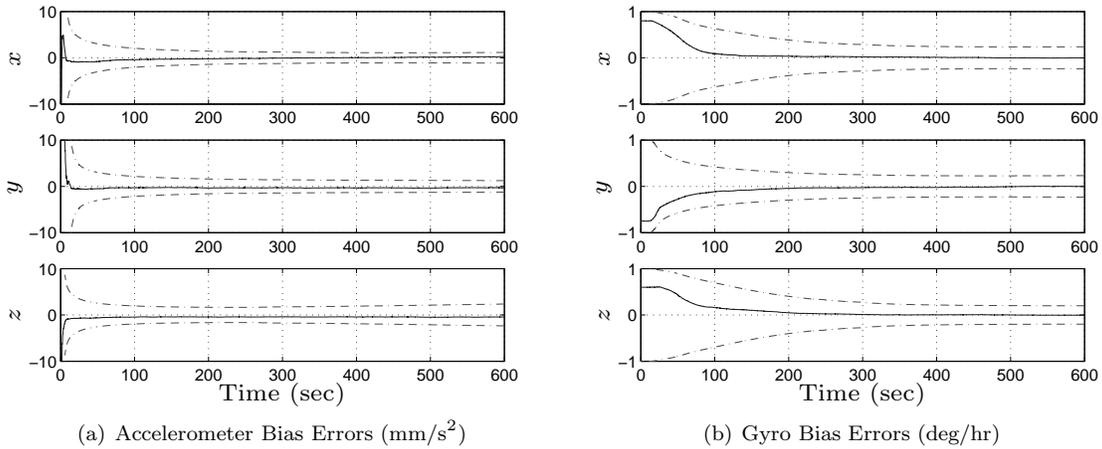(a) Accelerometer Bias Errors (mm/s^2)

(b) Gyro Bias Errors (deg/hr)

Figure 4. Bias Errors

errors are contained within 3σ bounds of 50 arc-seconds. All bias estimates are shown to converge quickly. These results clearly show that the derived relative equations provide a viable means to accurately estimate both relative attitude and position.

VI.   Path Trajectory Application

In this section an application of the previously derived filter equations is shown. Specifically, an optimal trajectory is designed to increase the observability of the relative position states with control applied to the follower. In practical applications, this type of maneuver would be applied between vehicle take-off and the arrival of the vehicles in their designated mission area. The purpose is to achieve the best possible relative position information before the mission begins. This task is assumed to be equivalent to improving the accuracy of the position estimates of the EKF developed in the prior sections. Optimal control techniques will be employed to design an optimal trajectory. It is assumed that this optimal path won't be used until after the primary state estimator has converged. This allows the bias states to be ignored for this development. Two types of control are possible, rotational control and translational control. In practical applications, the attitude of an air vehicle will be constrained by the desired direction of motion and the aerodynamics that govern its flight. For this reason, translational control will be the focus here. To keep this work from being tied to any specific air vehicle, only a generic translational control term will be used.

American Institute of Aeronautics and Astronautics

For future applications, the following development will need to be repeated with the chosen air vehicle's dynamics to ensure that the resulting trajectory is feasible.

The measure of an EKF's accuracy is defined by the 3σ bounds as given by the filter covariance matrix. The cost function will look to minimize the diagonal elements of the this matrix that correspond to the position states. In formulating the cost function, the information form of the covariance update will be used:[32]

$$(P_k^+)^{-1} = (P_k^-)^{-1} + H_k^T R_k H_k \tag{59}$$

The previously derived filter used a sequential update, allowing the above equation to be rewritten as

$$(P_k^+)^{-1} = (P_k^-)^{-1} + \sum_{i=1}^{n} \left(H_{ki}^T R_k H_{ki} \right) \tag{60}$$

$$\equiv (P_k^-)^{-1} + \sum_{i=1}^{n} \mathcal{B}_{ki} \tag{61}$$

The subscript i corresponds to the beacon number of the current Measurement, and n is the total number of beacons.

Minimizing the desired elements of the updated covariance P_k^+ requires maximizing its inverse, and thus maximizing the right hand side of Eq. (59). Since the propagated covariance P_k^- is given at each time step, maximizing the right hand side requires maximizing the summation of $\mathcal{B}_{ki}$.[20] Using Eq. (56) and the QUEST covariance to simplify the control design only (the navigation equations still used the generalized covariance model), the submatrix corresponding to the position elements is written as

$$\begin{bmatrix} \mathcal{B}_{ki}(4,4) & \mathcal{B}_{ki}(4,5) & \mathcal{B}_{ki}(4,6) \\ \mathcal{B}_{ki}(5,4) & \mathcal{B}_{ki}(5,5) & \mathcal{B}_{ki}(5,6) \\ \mathcal{B}_{ki}(6,4) & \mathcal{B}_{ki}(6,5) & \mathcal{B}_{ki}(6,6) \end{bmatrix} = \left(\frac{\partial \mathbf{b}_i}{\partial \mathbf{r}_{f|l}^f} \right)_i^T \left(\sigma^2 I_{3\times 3} \right) \left(\frac{\partial \mathbf{b}_i}{\partial \mathbf{r}_{f|l}^f} \right)_i$$

$$= \sigma^2 \left(\frac{\partial \mathbf{b}_i}{\partial \mathbf{r}_{f|l}^f} \right)_i^T \left(\frac{\partial \mathbf{b}_i}{\partial \mathbf{r}_{f|l}^f} \right)_i \tag{62}$$

with the diagonal elements of this matrix given by

$$\mathcal{B}_{ki}(4,4) = \frac{\sigma^2 \left[(Y_i + y)^2 + (Z_i + z)^2 \right]}{(\mathbf{R}_i + \mathbf{r}_{f|l}^f)^T (\mathbf{R}_i + \mathbf{r}_{f|l}^f)} \tag{63a}$$

$$\mathcal{B}_{ki}(5,5) = \frac{\sigma^2 \left[(X_i + x)^2 + (Z_i + z)^2 \right]}{(\mathbf{R}_i + \mathbf{r}_{f|l}^f)^T (\mathbf{R}_i + \mathbf{r}_{f|l}^f)} \tag{63b}$$

$$\mathcal{B}_{ki}(6,6) = \frac{\sigma^2 \left[(X_i + x)^2 + (Y_i + y)^2 \right]}{(\mathbf{R}_i + \mathbf{r}_{f|l}^f)^T (\mathbf{R}_i + \mathbf{r}_{f|l}^f)} \tag{63c}$$

Optimal control problems are generally stated in terms of minimizing a function. Therefore, maximizing $\sum_{i=1}^{n} \sum_{j=4}^{6} \mathcal{B}_{ki}(j,j)$ is accomplished by minimizing $(-1) \sum_{i=1}^{n} \sum_{j=4}^{6} \mathcal{B}_{ki}(j,j)$, which is written as

$$-\sum_{i=1}^{3} \sum_{j=4}^{6} \mathcal{B}_{ki}(j,j) = -\sum_{i=1}^{3} \frac{2\sigma^2}{(\mathbf{R}_i + \mathbf{r}_{f|l}^f)^T (\mathbf{R}_i + \mathbf{r}_{f|l}^f)} \tag{64}$$

A numerical problem can be seen by examining the denominator. Minimizing Eq. (64) requires the denominator to be made as small as possible. Its composition allows for it to achieve a zero value, which results in a numerical singularity. To avoid this difficulty a slightly different form of Eq. (64) will be used, given by $w_1 \sum_{i=1}^{n} (\mathbf{R}_i + \mathbf{r}_{f|l}^f)^T (\mathbf{R}_i + \mathbf{r}_{f|l}^f)$. This removes the mathematical singularity while still resulting in the same minimum. The constant coefficients have been replaced with a user specified weighting coefficient, w_1.

Another difficulty with this term is that its minimum requires the follower to be driven close to the leader. More specifically, the follower will asymptotically approach

$$\left(\mathbf{r}_{f|l}^f \right)_* = \frac{-1}{n} \sum_{i=1}^{n} \mathbf{R}_i \equiv \frac{-1}{n} \mathbf{R}_T \tag{65}$$

Physically, this means that the follower will asymptotically approach a relative position such that the mean beacon vector position will be located at the origin of the leader reference frame. In practical applications, this will likely cause a collision between the vehicles. To prevent such an occurrence, a state constraint will be imposed upon the system of the form

$$\|\mathbf{r}_{f|l}^f\| \geq r_{min} \tag{66}$$

where r_{min} is the minimum desired distance between the origins of the two vehicles body frames. For this constraint, it is assumed that the origins of the body frames are located at the geometric center of each vehicle. If this is not the case, the constraint needs to be modified appropriately.

The constraint can be appended into the loss function using a standard Lagrange multiplier approach.[33] However, a numerical solution to this optimization problem may be difficult to achieve. Here, a simpler method is used to impose the constraint, where an exponential is appended to the cost function, which now has the form of

$$
\begin{aligned}
J[\mathbf{x}(t), \mathbf{u}(t)] \;=\; & \int_{t_0}^{t_f} \left\{ \frac{1}{2} w_1 \sum_{i=1}^{n} (\mathbf{R}_i + \mathbf{r}_{f|l}^f(t))^T (\mathbf{R}_i + \mathbf{r}_{f|l}^f(t)) + \frac{1}{2} w_2 \left(\dot{\mathbf{r}}_{f|l}^f(t) \right)^T \dot{\mathbf{r}}_{f|l}^f(t) \right. \\
& \left. + \frac{1}{2} w_3 \left(\ddot{\mathbf{r}}_{f|l}^f(t) \right)^T \ddot{\mathbf{r}}_{f|l}^f(t) + w_4 \exp\left(k(r_{min} - \|\mathbf{r}_{f|l}^f(t)\|) \right) \right\} dt
\end{aligned}
\tag{67}
$$

where k is a user-specified coefficient and $\mathbf{u} \equiv \mathbf{a}_f^f = A_I^f \mathbf{a}_f^I$ is contained within the relative acceleration term. The primary goal of the follower during this calibration period is to perform the same maneuver as the leader. Since improving the observability is a secondary goal, the optimal trajectory should minimize deviations from that maneuver. This is why the relative velocity and relative acceleration are used instead of the follower velocity and follower acceleration.

The optimal control trajectory can be determined using standard unconstrained optimization methods, but choosing w_1 and w_4 independently may violate the constraint. The relation of the weight w_4 to w_1 is now shown. Equation (65) gives the minimum for an unconstrained system. Now, consider a constraint sphere of radius r_{min} about the leader upon which the follower is required to move. Because the cost function is based on the distance from the beacons to the leader, the cost function will vary over the constraint sphere as long as $\mathbf{R}_T$ is non-zero. If this value is zero, the optimal trajectory will simply be a straight line from the initial relative position to the closest point on the constraint sphere with the speed and acceleration determined by the relative weights. The optimal relative position will be that which forces $\mathbf{R}_T$ to be normal to the constraint sphere and pointing inward. Mathematically, this is written as

$$(\mathbf{r}_{f|l}^f)_* = -r_{min} \frac{\mathbf{R}_T}{\|\mathbf{R}_T\|} \tag{68}$$

Since this value is constant, the optimal relative velocity and acceleration are given by

$$(\dot{\mathbf{r}}_{f|l}^f)_* = \mathbf{0} \tag{69a}$$

$$(\ddot{\mathbf{r}}_{f|l}^f)_* = \mathbf{0} \tag{69b}$$

Knowing the desired location of the optimal position allows w_4 to be determined as a function of w_1. The optimal position occurs when $\frac{\partial J}{\partial \mathbf{x}} = \mathbf{0}$. Since the optimal relative velocity and relative acceleration are equal to zero, they aren't present in the following development. Working from Eq. (72), this partial derivative is given by

$$
\begin{aligned}
\frac{\partial J}{\partial \mathbf{x}} \;=\; & w_1 \sum_{i=1}^{n} (\mathbf{R}_i + \mathbf{r}_{f|l}^f)^T - k w_4 \exp\left(k(r_{min} - \|\mathbf{r}_{f|l}^f\|) \right) \frac{(\mathbf{r}_{f|l}^f)^T}{\|\mathbf{r}_{f|l}^f\|} \\
\;=\; & w_1 (\mathbf{R}_T + n\mathbf{r}_{f|l}^f)^T - k w_4 \exp\left(k(r_{min} - \|\mathbf{r}_{f|l}^f\|) \right) \frac{(\mathbf{r}_{f|l}^f)^T}{\|\mathbf{r}_{f|l}^f\|} \\
\;=\; & w_1 (\|\mathbf{R}_T\| - n\, r_{min}) \frac{(\mathbf{R}_T)^T}{\|\mathbf{R}_T\|} + k w_4 \exp\left(k(r_{min} - r_{min}) \right) \frac{(\mathbf{R}_T)^T}{\|\mathbf{R}_T\|} = \mathbf{0}^T
\end{aligned}
\tag{70}
$$

American Institute of Aeronautics and Astronautics

where the second line makes use of Eq. (68). Since the equation is solely a function of vectors along the direction of $\mathbf{R}_T$, the magnitudes alone are used to solve the equation for w_4. This yields

$$w_4 \;=\; \frac{w_1}{k}\left(n\,r_{min} - \|\mathbf{R}_T\|\right) \tag{71}$$

Use of this equation allows an optimization to be performed without the use of Lagrange multipliers to satisfy the inequality constraint. Equation (67) can then be written as

$$
\begin{aligned}
J[\mathbf{x}(t),\mathbf{u}(t)] \;=\; \int_{t_0}^{t_f} \Bigg\{ & \frac{1}{2} w_1 \sum_{i=1}^{n} (\mathbf{R}_i + \mathbf{r}_{f|l}^{f}(t))^T (\mathbf{R}_i + \mathbf{r}_{f|l}^{f}(t)) \\
& + \frac{1}{2} w_2 \left(\dot{\mathbf{r}}_{f|l}^{f}(t)\right)^T \dot{\mathbf{r}}_{f|l}^{f}(t) + \frac{1}{2} w_3 \left(\ddot{\mathbf{r}}_{f|l}^{f}(t)\right)^T \ddot{\mathbf{r}}_{f|l}^{f}(t) \\
& + \frac{w_1}{k}\left(n\,r_{min} - \|\mathbf{R}_T\|\right) \exp\left(k(r_{min} - \|\mathbf{r}_{f|l}^{f}(t)\|)\right) \Bigg\} dt
\end{aligned}
\tag{72}
$$

Even though the optimal position is known, it is still necessary to develop the trajectories that will maneuver the follower from its initial location to that position. Trajectories developed from this cost function will fall into one of two categories, which depend upon the location of the follower with respect to the constraint sphere and the constrained optimal position. If a direct path would require movement through the constraint sphere, the resulting optimal trajectory will drive the follower onto that sphere, and then follow a path along the sphere to the optimal position. Otherwise, the path will only be constrained by the user-specified weighting coefficients.

A. Simulation Results

This section shows simulation results of a maneuver using the previously developed optimal control law, along with several other trajectories to provide points of comparison. Three beacons have been determined to be the minimum required for continuous observability by simulations performed in Ref. 34. The first three beacons of Table 2 will therefore be used to generate the optimal trajectory. Once again, the number of beacons onboard the air vehicle will generally need to be higher to ensure that this minimum number always has clear lines of sight. For practical applications, a geometric analysis of the host vehicle structure, the possible locations of its beacons and the possible relative positions of the communicating vehicles will be required.

The other relevant parameters in developing the trajectory are a minimum distance of $r_{min} = 20$ meters and weights of $w_1 = 100$, $w_2 = 1$ and $w_3 = 40$. The value of r_{min} is chosen so that it would prevent collisions of larger air vehicles, such as the Predator which has a wingspan of approximately fifteen meters. When computing an optimal trajectory for smaller air vehicles, this constraint should be reduced appropriately. Weights for the cost function are chosen by balancing the desire for a quick approach to the optimal position with the need to prevent control inputs from becoming unrealistic. The above weights yield a trajectory that reasonably satisfies these competing factors.

Figure 5 shows the resulting optimal trajectory in NED coordinates. Each subplot shows two lines. The solid line corresponds to the computed true trajectory, while the dashed line corresponds to the optimal position. Initially, all three position components move towards their respective optimal positions. After about five seconds, the y component then begins to increase. This is due to the fact that both the x and z components have to cross zero in order to reach their optimal positions. In order for the minimum distance constraint to be maintained, the y position must increase. It is this type of feature that requires an optimal trajectory to be calculated. If the follower just traveled straight towards the optimal position, there is a chance that the constraint will be violated resulting in a possible collision.

Two additional trajectories are tested for comparison. They are given by the following equations:

$$
\mathbf{r}_{f|l}^{N}(\text{constant}) = \begin{bmatrix} 60 \\ 40 \\ 70 \end{bmatrix} \text{ meters} \tag{73a}
$$

$$
\mathbf{r}_{f|l}^{N}(\text{sinusoid}) = \begin{bmatrix} 30\sin(2\pi t/600) + 60 \\ 20\sin(2\pi t/600) + 40 \\ 40\sin(2\pi t/600) + 70 \end{bmatrix} \text{ meters} \tag{73b}
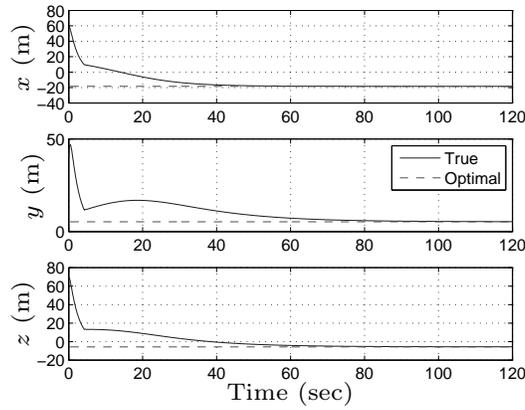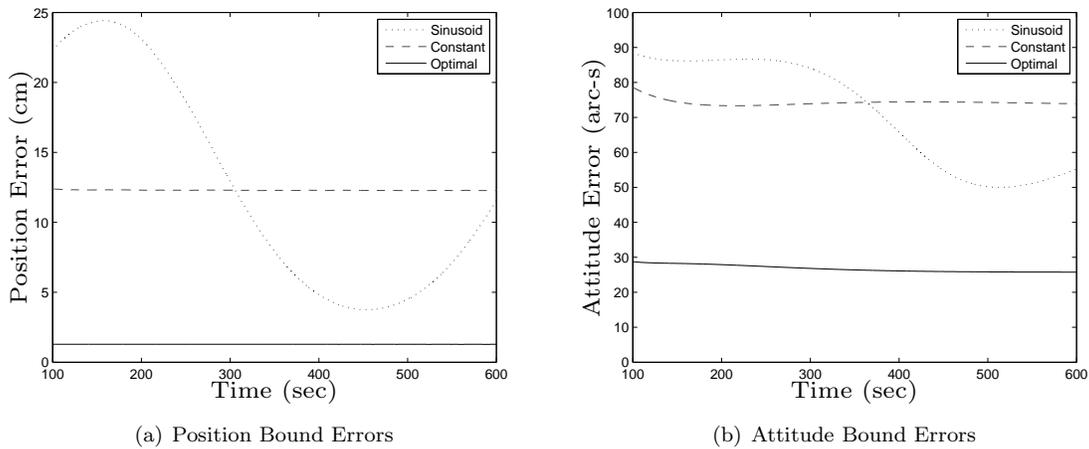$$

Figure 5. Optimal Relative Position Trajectory

| (a) Position Bound Errors | (b) Attitude Bound Errors |

Figure 6. Error Bound Comparison

To provide an accurate comparison, they begin with the same relative position, relative velocity and relative attitude as that of the optimal trajectory. A calibration maneuver has been assumed to already take place before the optimal control law is invoked. Therefore, the initial conditions of the biases are set to their respective true values, and the initial covariances of the gyro and accelerometer biases are set to 3σ bounds 0.3 deg/hr and 0.3 mm/s^2, respectively. Norms of the error bounds for both the relative position and relative attitude states are shown in Fig. 6. Significant increases in accuracy are seen when using the optimal trajectory when compared to the constant and sinusoidal trajectories. It should be noted that an improvement in attitude estimation accuracy is also achieved even though the optimization is performed with respect to the position components. This is a result of the coupling between the two sets of states through the LOS measurements.

Conclusions

The relative navigation equations for a pair of air vehicles were developed. An extended Kalman filter was then derived for estimation of relative position and attitude. Line-of-sight measurements are taken by simulating visual navigation beacons, which are assumed to be placed on the follower while the focal plane arrays are on board the leader. Simulation results demonstrated that the gyro and accelerometer biases can be estimated using a calibration maneuver. An optimal controller has also been developed to generate a trajectory which improves the estimation accuracy for a two vehicle system containing three visual navigation

American Institute of Aeronautics and Astronautics

beacons. This was accomplished by including the appropriate terms of the covariance update equation within the cost function. A state constraint is also included, which sets a lower bound on the norm of the relative position vector. The extended Kalman filter was tested on the optimal trajectory along with two additional trajectories. Simulations showed that accurate position and attitudes can be estimated, and that an optimal trajectory exists which results in significantly reduced covariance bounds for both the relative position and relative attitude states.

Acknowledgement

References

[1] Connelly, J., Kourepenis, A., Marinis, T., and Hanson, D., "Micromechanical Sensors in Tactical GN&C Applications," *AIAA Guidance, Navigation and Contol Conference*, Montreal, QB, Canada, Aug. 2001, AIAA-2001-4407.

[2] MacSween-George, S. L., "Will the Public Accept UAVs for Cargo and Passenger Transportation?" *Proceedings of the IEEE Aerospace Conference*, Vol. 1, IEEE Publications, Piscataway, NJ, 2003, pp. 357–367.

[3] Sarris, Z., "Survey of UAV Applications in Civil Markets," *The 9th Mediterranean Conference on Control and Automation*, Dubrovnik, Croatia, June 2001, ISBN 953-6037-35-1, MED01-164.

[4] DeGarmo, M. and Nelson, G., "Prospective Unmanned Aerial Vehicle Operations in the Future National Airspace System," *AIAA 4th Aviation Technology, Integration and Operations (ATIO) Forum*, Chicago, IL, Sept. 2004, AIAA-2004-6243.

[5] Ryan, A., Zennaro, M., Howell, A., Sengupta, R., and Hedrick, J. K., "An Overview of Emerging Results in Cooperative UAV Control," *Proceedings of the 43th IEEE Conference on Decision and Control*, Vol. 1, IEEE Publications, Piscataway, NJ, 2004, pp. 602–607.

[6] Johnson, E. N., Calise, A. J., Sattigeri, R., Watanabe, Y., and Madyastha, V., "Approaches to Vision-Based Formation Control," *Proceedings of the 43th IEEE Conference on Decision and Control*, Vol. 2, IEEE Publications, Piscataway, NJ, Dec. 2004, pp. 1643–1648.

[7] Aidala, V. J. and Hammel, S. E., "Utilization of Modified Polar Coordinates for Bearings-Only Tracking," *IEEE Transactions on Automatic Control*, Vol. 28, No. 3, March 1983, pp. 283–294.

[8] Chatfield, A. B., *Fundamentals of High Accuracy Inertial Navigation*, chap. 9, American Institute of Aeronautics and Astronautics, Inc., Reston, VA, 1997.

[9] Crassidis, J. L., "Sigma-Point Kalman Filtering for Integrated GPS and Inertial Navigation," *IEEE Transactions on Aerospace and Electronic Systems*, Vol. 42, No. 2, April 2006, pp. 750–756.

[10] Gustafsson, F., Gunnarsson, F., Bergman, N., Forssell, U., Jansson, J., Karlsson, R., and Nordlund, P.-J., "Particle Filters for Positioning, Navigation, and Tracking," *IEEE Transactions on Signal Processing*, Vol. 50, No. 2, Feb. 2002, pp. 425–435.

[11] Felter, S. C. and Wu, N. E., "A Relative Navigation System for Formation Flight," *IEEE Transactions on Aerospace and Electronic Systems*, Vol. 33, No. 3, July 1997, pp. 958–967.

[12] Woo, M. J. and Choi, J. W., "A Relative Navigation System for Vehicle Platooning," *Proceedings of the 40th SICE Annual Conference*, IEEE Publications, Piscataway, NJ, July 2001, pp. 28–31.

[13] Fosbury, A. M. and Crassidis, J. L., "Kalman Filtering for Relative Inertial Navigation of Uninhabited Air Vehicles," *AIAA Guidance, Navigation, and Control Conference*, Keystone, CO, Aug. 2006, AIAA-2006-6544.

[14] Mayo, R. A., "Relative Quaternion State Transition Relation," *Journal of Guidance, Navigation and Control*, Vol. 2, No. 1, Jan-Feb. 1979, pp. 44–48.

[15] Junkins, J. L., Hughes, D. C., Wazni, K. P., and Pariyapong, V., "Vision-Based Navigation for Rendezvous, Docking and Proximity Operations," *22nd Annual AAS Guidance and Control Conference*, Breckenridge, CO, Feb. 1999, AAS-99-021.

[16] Alonso, R., Crassidis, J. L., and Junkins, J. L., "Vision-Based Relative Navigation for Formation Flying of Spacecraft," *AIAA Guidance, Navigation, and Control Conference*, Denver, CO, Aug. 2000, AIAA-00-4439.

[17] Kim, S. G., Crassidis, J. L., Cheng, Y., Fosbury, A. M., and Junkins, J. L., "Kalman Filtering for Relative Spacecraft Attitude and Position Estimation," *Journal of Guidance, Control, and Dynamics*, Vol. 30, No. 1, Jan.-Feb. 2007, pp. 133–143.

[18] Valasek, J., Gunnam, K., Kimmett, J., Junkins, J. L., Hughes, D., and Tandale, M. D., "Vision-Based Sensor and Navigation System for Autonomous Air Refueling," *Journal of Guidance, Control, and Dynamics*, Vol. 28, No. 5, Sept.-Oct. 2005, pp. 979–989.

[19] Tandale, M. D., Bowers, R., and Valasek, J., "Robust Trajectory Tracking Controller for Vision Based Autonomous Aerial Refueling of Unmanned Aircraft," *Journal of Guidance, Control, and Dynamics*, Vol. 29, No. 4, July-Aug. 2006, pp. 846–857.

[20] Watanabe, Y., Johnson, E. N., and Calise, A. J., "Optimal 3-D Guidance from a 2-D Vision Sensor," *AIAA Guidance, Navigation and Control Conference*, Providence, RI, Aug. 2004, AIAA-2004-4779.

[21] Farrell, J. and Barth, M., *The Global Positioning System and Inertial Navigation*, chap. 2, McGraw-Hill, New York, NY, 1998.

[22] Shuster, M. D., "A Survey of Attitude Representations," *Journal of the Astronautical Sciences*, Vol. 41, No. 4, Oct.-Dec. 1993, pp. 439–517.

[23]Schaub, H. and Junkins, J. L., *Analytical Mechanics of Aerospace Systems*, American Institute of Aeronautics and Astronautics, Inc., New York, NY, 2003, pp. 72–78.

[24]Lefferts, E. J., Markley, F. L., and Shuster, M. D., "Kalman Filtering for Spacecraft Attitude Estmation," *Journal of Guidance, Control, and Dynamics*, Vol. 5, No. 5, Sept.-Oct. 1982, pp. 417–429.

[25]Crassidis, J. L., "Sigma-Point Kalman Filtering for Integrated GPS and Inertial Navigation," *AIAA Guidance, Navigation, and Control Conference*, San Francisco, CA, Aug. 2005, AIAA-05-6052.

[26]Fosbury, A. M., *Control of Relative Attitude Dynamics of a Formation Flight Using Model-Error Control Synthesis*, Master's thesis, University at Buffalo, State University of New York, March 2005.

[27]Van-Loan, C. F., "Computing Integrals Involving Matrix Exponentials," *IEEE Transactions on Automatic Control*, Vol. AC-23, No. 3, Jun. 1978, pp. 396–404.

[28]Light, D. L., "Satellite Photogtammetry," *Maunual of Photogrammetry*, edited by C. C. Slama, chap. 17, American Society of Photogrammetry, Falls Church, VA, 4th ed., 1980.

[29]Shuster, M. D., "Kalman Filtering of Spacecraft Attitude and the QUEST Model," *Journal of the Astronautical Sciences*, Vol. 38, No. 3, July-Sept. 1990, pp. 377–393.

[30]Shuster, M. D. and Oh, S. D., "Three Axis Attitude Determination from Vector Observations," *Journal of Guidance, Navigation and Control*, Vol. 4, No. 1, Jan-Feb. 1981, pp. 70–77.

[31]Cheng, Y., Crassidis, J. L., and Markley, F. L., "Attitude Estimation for Large Field-of-View Sensors," *Journal of the Astronautical Sciences*, Vol. 54, No. 3-4, July-Dec. 2006, pp. 433–448.

[32]Crassidis, J. L. and Junkins, J. L., *Optimal Estimation of Dynamic Systems*, chap. 5, Chapman & Hall/CRC, Boca Raton, FL, 2004.

[33]Bryson, A. E., *Dynamic Optimization*, chap. 9, Addison Wesley Longman, Menlo Park, CA, 1999.

[34]Fosbury, A., *Control and Kalman Filtering for the Relative Dynamics of a Formation of Uninhabited Autonomous Vehicles*, Ph.D. thesis, University at Buffalo, State University of New York, August 2006.